2023 CCM & IMEKO TC16 7th International Conference on Pressure and Vacuum Metrology
IMEKO TC-16 2023
Washington DC, U.S.A., May 15-19, 2023

Primary Sound Standard based on Dynamic Fabry-Pérot Refractometry

Akobuije Chijioke, Richard A. Allen, Steven E. Fick, Benjamin J. Reschovsky, Jared H. Strait and Randall P. Wagner

National Institute of Standards and Technology, Gaithersburg, MD 20899, USA. email: akoc@nist.gov

***Abstract* – We describe an optical sound standard in which the sound pressure is measured by using a high-finesse optical cavity to observe the induced change in the refractive index of the medium (acousto-optic effect). The optical refractive index of a substance varies with density, and for a compressible substance it will therefore vary in time in an acoustic field. To accurately measure the refractive index changes due to acoustic density variations, we enhance the induced optical phase shifts using a high-finesse optical cavity. By tracking the shift in the optical cavity resonance frequency we sensitively track the shift of the refractive index of the cavity medium and thereby the acoustic pressure in the cavity. We perform the optical measurement at standard telecom wavelength (1550 nm), thereby minimizing the cost of the optoelectronic components required. We report initial measurements in an acoustic resonator, comparing the pressure indicated by the optical cavity to the pressure indicated by a condenser microphone, at 1 kHz and 2 kHz acoustic frequencies.**

I. INTRODUCTION

In the past decade, the development of primary pressure measurement based on Fabry-Pérot refractometry has constituted a sea change in the field of pressure metrology. In the field of acoustics, refractivity-based sound sensing has been explored [1,2], but the accuracy (including sensitivity) to be competitive with established calibration methods has not been demonstrated. We propose applying Fabry-Perot refractometry, which has been successfully developed for absolute static pressure metrology [3,4], to measurements of acoustic pressure, which is a small amplitude (typically < 100 Pa) pressure variation riding on the mean (typically ≈ 101 kPa) ambient pressure. Acoustic frequencies of interest in air range from millihertz (infrasound) frequencies through the audible region spanning the frequency range 20 Hz to 20 kHz, up to ultrasonic frequencies exceeding 1 MHz. In contrast to static (absolute) pressure metrology, the measurement of acoustic pressure is based on the pressure derivative of the refractive index rather than its absolute value. In the infrasonic frequency range the system design can follow static pressure metrology approaches quite closely, and we have recently learned of work along these lines [5]. The work we describe in this paper has so far been developed with the audible frequency range in mind.

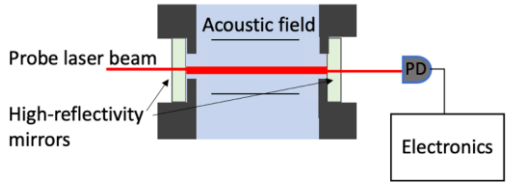

Fig. 1. Measurement concept: an acoustic field exists in a fluid medium between two stationary high-reflectivity mirrors, aligned to create an optical cavity. A laser is used to measure changes in the optical properties of the cavity (e.g. resonance frequency) due to acoustically-driven changes in the optical refractive index of the fluid.

II. MEASUREMENT METHOD

A. Refractive index dependence on sound

Acousto-optic sound detection is based on the variation of the optical refractive index of a fluid with density [3,4]. In a sound wave the density, pressure, temperature and refractive index all vary, and for a single tone this is a sinusoidal variation at the acoustic frequency. These variations are small ($< 10^{-3}$) relative variations at typical (< 100 Pa) acoustic pressure amplitudes under standard atmospheric conditions, and the derivative of the refractive index with pressure $\frac{dn}{dp}$ allows the acoustic pressure amplitude to be inferred from the observed amplitude of variation of the refractive index. At acoustic frequencies in air and away from boundaries the acoustic compression of the air is adiabatic to high accuracy. In other words, inferring the pressure amplitude from the refractive index amplitude requires the effect of the temperature change to

be taken into account

$$\left(\frac{dn}{dp}\right)_A = \left(\frac{dn}{dp}\right)_T + \left(\frac{dn}{dT}\right)_p \left(\frac{dT}{dp}\right)_A \qquad (1)$$

For air, $\left(\frac{dn}{dp}\right)_T$ and $\left(\frac{dn}{dT}\right)_p$ are available from published empirical refractive index dependence on environmental parameters [6,7], and for a given wavelength are functions of temperature, pressure and air composition (in particular relative humidity and CO_2 concentration). Their approximate values at 20 °C and 101.325 kPa are 2.65×10^{-9} Pa^{-1} and -9.39×10^{-7} K^{-1}. We can obtain $\left(\frac{dT}{dp}\right)_A$ from the following thermodynamic identity for a simple substance without sources of entropy change other than heat transfer:

$$\left(\frac{dT}{dp}\right)_A = \frac{T}{c_P}\left(\frac{\partial v}{\partial T}\right)_P \qquad (2)$$

where c_P is the specific heat at constant pressure and v is the specific volume. For an ideal gas this simplifies to

$$\left(\frac{dT}{dp}\right)_A = \frac{\gamma-1}{\gamma}\frac{T}{P}\,, \qquad (3)$$

where γ is the ratio of constant volume specific heat to constant pressure specific heat and is a function of temperature. Using (3) we obtain $\left(\frac{dT}{dp}\right)_A = 8.48 \times 10^{-4}$ K/Pa at 20 °C and 101.325 kPa. The second term on the right hand side of (1) is thus has a magnitude about 30 % that of the first term and the opposite sign. By using tabulated [8] equation of state data in (2), we estimate that the true value of $\left(\frac{dT}{dp}\right)_A$ for air differs from the ideal gas approximation by around 0.3 %, so that using the ideal gas approximation introduces an uncertainty of 0.1 % in the refractive index derivative $\left(\frac{dn}{dp}\right)_A$. The uncertainty in $\left(\frac{dn}{dp}\right)_A$ is easily reduced by using accurate equation of state data to evaluate $\left(\frac{dT}{dp}\right)_A$. A more fundamental approach to obtaining $\left(\frac{dn}{dp}\right)_A$ is to start with the virial Lorentz-Lorenz equation,

$$\frac{n^2-1}{n^2+2} = A_R\rho_v + B_R{\rho_v}^2 + O({\rho_v}^3), \qquad (4)$$

where ρ_v is the particle number density, A_R is the molecular polarizability, and B_R is the second refractive virial coefficient, and to take the derivative of this with respect to density. This approach has advantages, especially for the case where the acoustic medium is a pure substance (e.g. nitrogen), however we will not discuss it further here.

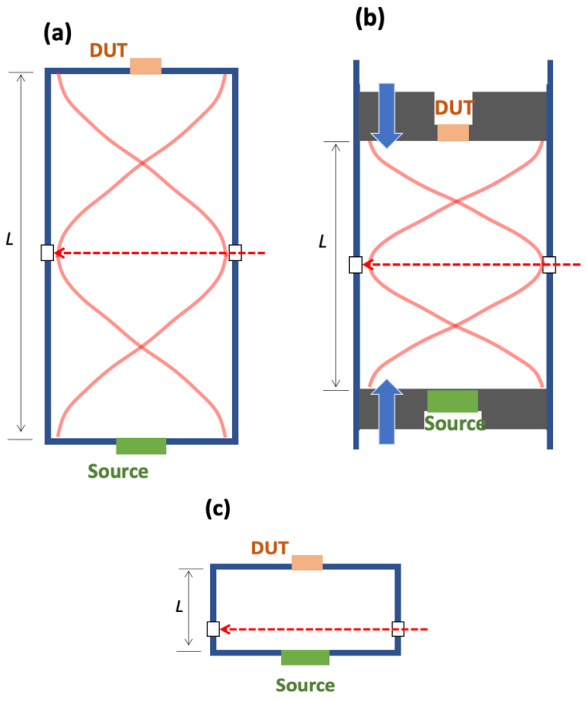

Fig. 2. Acoustic cavity types. (a) Acoustic resonator, in which plane standing wave resonances are supported at acoustic frequencies that are integer multiples of the fundamental frequency $c_s/2L$, where c_s is the speed of sound. For such standing waves, an optical cavity located at the midpoint along the resonator length sees the same acoustic pressure as the two ends of the resonator. The solid red lines illustrate the relative acoustic pressure distribution in the second longitudinal plane wave mode of the resonator. (b) Adjustable length resonator, in which the acoustic frequencies of the plane standing wave resonances can be continuously adjusted over a wide range. (c) Acoustic "coupler", which has dimensions small compared to the acoustic wavelengths of interest, such that the acoustic field can be considered as spatially uniform inside the coupler.

B. Enhanced acousto-optic measurement in an optical cavity.

The phase change ϕ of light of wavelength λ over distance l in a medium of refractive index n is

$$\phi = n\, l\, \frac{2\pi}{\lambda}\,. \qquad (5)$$

Thus, perturbations δl and δn in the distance and index respectively cause a phase perturbation $\delta\phi$ of

$$\delta\phi = (n\,\delta l + l\,\delta n)\,\frac{2\,\pi}{\lambda}. \qquad (6)$$

The dependence of the refractive index of the medium on density thus leads to a time-varying optical phase shift induced by the time-varying density in the acoustic field, which can be used to measure the sound level. The change in index may vary along the optical path, and the observed index-driven optical phase change is the path-integrated value. For a high sensitivity $\frac{d\phi}{dp}$ of the phase with respect to acoustic pressure, the distance l over which the index changes and is probed by the light should be maximized,

$$\frac{d\phi}{dP} = \frac{2\,\pi}{\lambda}\,l\,\frac{dn}{dp}. \qquad (7)$$

Making l large is essentially what a high-finesse optical cavity accomplishes. The effective optical path length is increased by a factor equal to the cavity finesse. The optical phase change can conveniently be read out as the resulting change in cavity resonance frequency ν_r

$$\nu_r\delta\nu_r = -\nu_r\left(\frac{\delta l}{l} + \frac{\delta n}{n}\right), \qquad (8)$$

where the cavity resonance frequency is on the order of 10^{14} Hz for visible and near-infrared light. The sensitivity of the output signal to the acoustic pressure is

$$\frac{d\nu_r}{dp} = -\nu_r\left(\frac{1}{n}\frac{dn}{dp} + \frac{1}{l}\frac{dl}{dp}\right). \qquad (9)$$

In equations (8) and (9) the equivalence of relative length and refractive index changes is clear. Any change in the cavity length at the acoustic frequency, for instance due to deformations driven by the acoustic pressure, will cause an error unless it is accounted for.

C. Acoustic field configurations

In order to use this method to perform acoustic pressure calibration of microphones, the acoustic pressure in the optical cavity must be the same as (or have a known relationship to) that seen by the microphone. Two alternative arrangements for achieving this are shown in Figure 2. In a cylindrical acoustic resonator, shown in Figures 2a and 2b, an acoustic standing wave is used to create an acoustic field in which the acoustic pressure is nearly the same at the optical cavity location as at the location where the microphone is placed, e.g., an end face of a cylindrical tube resonator. In an acoustic coupler, shown in Figure 2c, the enclosed volume of the sound field is sufficiently small in comparison to the acoustic wavelength that a uniform sound pressure can be assumed.

D. Design parameters

In the second column of Table 1 we list characteristic parameters for an acoustic-resonator-based configuration operating in the audio frequency range with air.

Table 1. Typical values of system parameters for an acoustic resonator based system, and realized values of parameters in initial experimental measurements.

Parameter	Typical Value	Initial Experiment
Refractive index pressure dependence (air), $\left(\frac{1}{n}\frac{dn}{dP}\right)_A$	1.9×10^{-9} Pa^{-1}	1.9×10^{-9} Pa^{-1}
Acoustic pressure amplitude	10 Pa	2 Pa to 21 Pa
Acoustic resonator length	0.345 m	0.3447 m
Acoustic frequency	1 kHz	1 kHz, 2 kHz
Optical wavelength	1 µm	1550 nm
Cavity resonance frequency shift	3.6 MHz	1 MHz to 11 MHz
Cavity finesse	10 000	12 000
Cavity length	100 mm	124 mm
Cavity linewidth	150 kHz	100 kHz
Estimated acoustic pressure detection sensitivity*	0.084 % (0.0073 dB)	

**based on on assumed lock accuracy of 2 % of linewidth*

III. EXPERIMENTAL SYSTEM

A. Acoustic resonator

The acoustic resonator we have constructed is illustrated in Figure 3. It is designed for use in air or nitrogen, and has a length (at 20 °C) of 344.69 mm ± 0.02 mm, thus supporting plane-wave acoustic resonances at multiples of approximately 500 Hz. The length is chosen for operation of the resonator at 1000 Hz, which is a cardinal acoustical calibration frequency. The even plane wave resonances occur at 1000 Hz and integer multiples thereof, and for these the acoustic pressure amplitude and phase are the same at the resonator midplane and ends. An optical cavity spanning the diameter of the resonator at its midplane thus measures nearly the same pressure as seen by a microphone diaphragm mounted flush in one of the ends of the resonator. We discuss the small difference in the pressure at these two locations in section IIIB below. The acoustic pressure standing wave in the resonator is generated by a piezoelectric film disc sandwidched in one of the resonator endplates. Thermal tuning (e.g. within a range of ≈ 1 K) of the gas temperature may be used to finely adjust the acoustic resonant frequencies if it is desired to operate at exact frequencies.

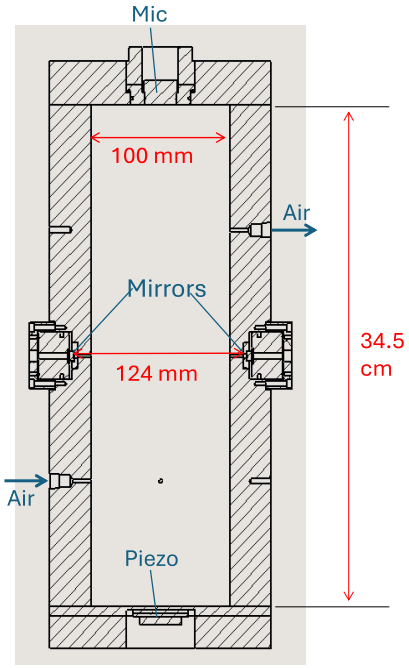

Fig. 3. Scale diagram of constructed acoustic resonator, showing locations of mirrors, piezoelectric disk sound source, microphone under test, and holes.

The resonator is made of stainless steel, and has an inner diameter of 100 mm and a wall thickness of 30 mm. The diameter is large enough to provide a sufficiently high cavity finesse for the given mirror reflectivities. The wall thickness is sufficient to limit the optical cavity relative length oscillation at the acoustic frequency due to radial "breathing"-type deformation of the acoustic resonator driven by the acoustic pressure to ≈ 0.7 % - 0.8 % of the relative refractive index change, at frequencies in the range 500 Hz - 3 kHz (e.g. the relative cavity length change at 1 kHz is estimated as 1.4×10^{-11} Pa^{-1}). This estimate was obtained by modeling the structural frequency response of the resonator to internal acoustic pressure using the COMSOL[9,10] finite element analysis software package. We estimate that with such simulation we can model the cavity length oscillation due to the overall acoustic resonator deformation in this frequency range to within 20 % ($k = 2$) relative uncertainty, which would result in a contribution of ≤ 0.2 % to the final acoustic pressure uncertainty. However we intend to perform direct measurement of the mirror motion using accelerometers mounted on the cavity mirrors or laser vibrometry.

B. Optical cavity

Our optical cavity is designed for use with ≈ 1550 nm laser light (telecom wavelength), for which optoelectronic components are conveniently available. It has a length of 124 mm, consisting of the 100 mm inner diameter of the acoustic resonator plus a 12 mm long, 2 mm diameter recess hole in front of each mirror. The free spectral range of the optical cavity is thus $\Delta\nu_{FSR} = c/2nL_{\mathrm{oc}} = 1.208$ GHz, where c is the vacuum speed of light, n is the refractive index of the medium and L_{oc} is the optical cavity length. The mirrors have a nominal power reflectivity of 0.9999 at a central wavelength of 1600 nm, which would yield a finesse of 31420 corresponding to a cavity resonance linewidth of 38.5 kHz. In practice we have observed a linewidth of ≈ 100 kHz corresponding to a finesse of 12 000. The factor of 3 reduction in finesse could be due to operation of the mirrors ≈ 50 nm off their design wavelength, and/or to increased losses due to aperture effects or surface contamination.

As discussed above in section IIIA, the resonator is designed to minimize its radial deformation in response to the internal acoustic pressure. The optical cavity length oscillation is not due only to deformation of the acoustic resonator, but also to any relative motion of the mirrors with respect to the acoustic resonator body (or more precisely, the differential component of such relative motion along the longitudinal axis of the optical cavity). The system is therefore designed with robust and stiff mounting of the mirrors. However, mirror alignment difficulties with our initial design prevented us from mounting the mirrors as intended, resulting in the mirrors being held in place only by a few (4) spots of epoxy [11] at their peripheral surfaces. We do not have an accurate estimate of the stiffness of this mounting, nor of the mirror motion relative to the resonator body with the mirrors mounted in this manner. We suspect that due to such motion the cavity length oscillation in initial measurements was significantly larger than the component due to deformation of the acoustic resonator. As already mentioned, we intend to perform direct measurement of the mirror motion using accelerometers mounted on the cavity mirrors or laser vibrometry, and this measurement will include the effect of mirror motion relative to the resonator as well as the effect of deformation of the resonator.

The acoustic pressure amplitude is altered in the 2mm diameter holes between the mirror front surfaces and the main resonator volume, leading to a difference of up to ≈ 2 % between the average acoustic pressure along the optical cavity axis and the average acoustic pressure on the microphone surface, as evaluated by finite element modeling at 1 kHz and 2 kHz acoustic frequencies. The dependence of the acoustic pressure difference betweeen the two locations on the accuracy of the thermoviscous aspects of the acoustic modeling performed leads to an uncertainty contribution [$k = 2$] of 0.1 % and 0.5 % to the optically measured pressure at 1 kHz and 2 kHz respectively.

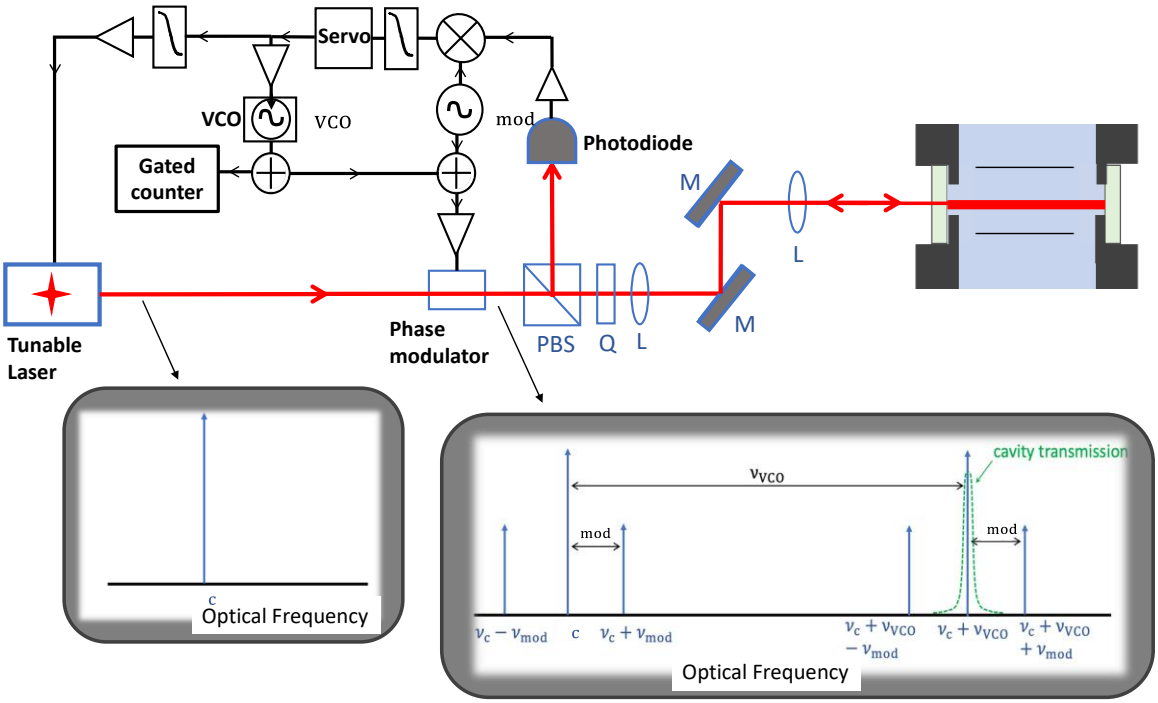

Fig. 4. Optical cavity resonant frequency readout scheme. Phase modulation of the laser light at two frequencies creates multiple sets of sidebands. Initial adjustment of the laser frequency brings one of these sets of sidebands close to a cavity TEM00 mode resonant frequency. A Pound-Drever-Hall lock with fast feedback to the laser frequency via a voltage controlled oscillator (VCO) and slow feedback via the laser current keeps the laser locked to the optical cavity. A gated frequency counter with a repetition rate of tens of kHz is used to sample the VCO frequency rapidly enough to track the cavity resonant frequency oscillation at the acoustic frequency. Not shown: a portion of the laser output is diverted to a wavemeter to measure the laser wavelength. PBS: polarizing beam splitter, Q: quarter-wave plate, M: mirror, L: lens.

C. Cavity resonant frequency readout

We sample the cavity resonant frequency ν_r at a rate greater than twice the acoustic frequency, allowing us to determine the amplitude of cavity resonant frequency oscillation. As illustrated in Figure 4, we use a dual sideband locking [12] variation of the Pound-Drever-Hall (PDH) approach [13, 14]. The frequency of the light incident on the optical cavity is modulated by driving a phase modulator with a signal that is the sum of two frequency components: an approximately 150 MHz "offset" signal ν_{VCO} that is generated by a voltage-controlled oscillator, and a 5 MHz "modulation" signal ν_{mod} that is generated by a fixed-frequency signal generator. This modulation generates families of frequency components (sidebands) in the laser light which are offset from the laser carrier frequency ν_{c} by $\pm N\nu_{\mathrm{VCO}} \pm M\nu_{\mathrm{mod}}$ where $N, M = 0,1,2,\ldots$. We use slow current-driven adjustment of the diode laser carrier frequency to bring the $N = 1, M = 0$ sideband in resonance with the optical cavity. The light reflected from the cavity is incident on a photodiode and demodulation at the modulation frequency generates a PDH error signal [13,14]. Feedback of the amplified error signal to the VCO keeps this sideband in resonance with (i.e. "locked to") the optical cavity as the cavity resonance frequency oscillates at the acoustic frequency, where the lock bandwidth and dynamic range must be sufficient to track this oscillation. We use a gated frequency counter with a repetition rate of tens of kHz (Keysight model 53230A) to make several measurements of ν_{VCO} per acoustic cycle, allowing us to extract the oscillating refractive index and thereby the acoustic pressure.

D. Summary

In the third column of Table 1 we list parameters for our experimental implementation of a Fabry-Pérot cavity sound standard using an acoustic resonator.

IV. INITIAL MEASUREMENTS

With such a system we have made an initial rapid comparison of the optically measured sound pressure level in air to the sound pressure levels indicated by a Brüel & Kjær type 4144 condenser microphone, at acoustic

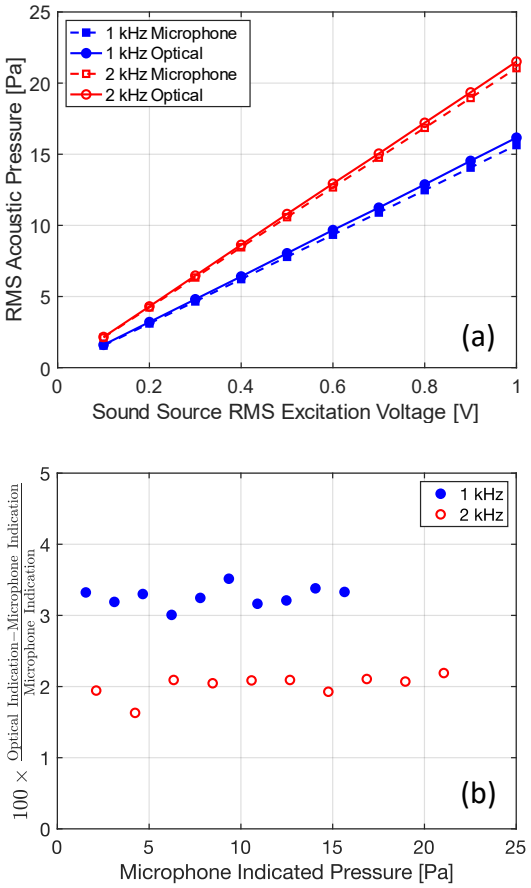

Fig. 5. Results of comparing sound pressure level indicated by Brüel & Kjær type 4144 microphone (Ser. No. 473977) with the optically measured sound pressure level based on refractive index change. The microphone had been calibrated to an uncertainty (k=2) of a few percent.

frequencies of 1 kHz and 2 kHz. The measurements were made under uncontrolled indoor laboratory conditions (T = 22.5 °C ± 4.5 °C, P = 102.1 kPa ± 0.5 kPa, RH = 50 % ± 30 %). The microphone measurement system was calibrated with a pistonphone and its uncertainty (k = 2) was on the order of a few percent. As discussed in section IIIB, the optical cavity mirrors were not robustly mounted to the resonator body for these initial measurements. The mirror displacement amplitude at the acoustic frequency was expected to be larger than that due to resonator breathing, but has not been measured and is essentially unknown.

The results of this comparison are shown in Figure 5. Differences between the optical measurement and the microphone indication were less than 4 % (0.34 dB). Given the manner of the optical cavity mirror mounting and the unknown mirror motion relative to the resonator body, the agreement is better than expected. The measurements suggest that the displacement of each mirror relative to half the optical cavity length was less than 10 % of the relative refractive index change.

V. SUMMARY AND OUTLOOK

In summary, we have designed and assembled a system to measure acoustic pressure based on Fabry-Pérot refractometry, and to use this measurement to calibrate acoustic devices. In an initial study, we compared the optically measured acoustic pressure to the acoustic pressure indicated by a condenser microphone. Despite deficient mirror mounting and suspected errors due to mirror motion, fairly good agreement was observed between the optical pressure measurement and the microphone.

In our next measurements we plan to address the mirror motion error and uncertainty by both improving the mirror mounting and performing measurements of the mirror displacement in response to acoustic pressure in the resonator. We also plan to redesign the acoustic resonator (or coupler) to reduce or eliminate the holes between the mirror front surfaces and the main volume of the resonator/coupler, and to use a more-accurately calibrated microphone for the comparison.

We also plan to switch from air to pure nitrogen as the acoustic medium, for increased accuracy. We additionally plan to make measurements in helium, for direct quantum traceability [15].

REFERENCES

[1] K. Nakamura, M. Hirayama, and S. Ueha, *2002 IEEE Ultrason. Symp., vol. 1*, 609-612 (2002).

[2] A. Torras-Rosell, S. Barrera-Figueroa, and F. Jacobsen, *J. Acoust. Soc. Am.* **13**, 3786-3793 (2012).

[3] P. F. Egan, J. A. Stone, J. H. Hendricks, J. E. Ricker, G. E. Scace, and G. F. Strouse, *Opt. Lett.* **40**, 3945 (2015).

[4] P. F. Egan, J. A. Stone, J. E. Ricker, and J. H. Hendricks, *Rev. Sci. Instrum.* **87**, 053113 (2016).

[5] A. Rezki, Z. Silvestri, J-P. Wallerand, C. Guianvarc'h and M. Himbert, "Low-frequency acoustic pressure measurements based on a Fabry-Perot Refractometer", *IMEKO 24th TC3, 14th TC5, 6th TC16 and 5th TC22 International Conference*, 11-13 October 2022, Cavtat-Dubrovnik, Croatia. (2022).

[6] P. E. Ciddor, *Applied optics*, **35**, 1566-1573 (1996).

[7] K. P. Birch and M. J. Downs, *Metrologia* **31**, 315-316 (1994).

[8] D. R. Lide, ed. *CRC handbook of chemistry and physics*. Vol. 85. CRC press, 2004.

[9] *COMSOL Multiphysics*, COMSOL Ab., Stockholm, Sweden. Version 5.6 used.

[10] Certain commercial items are identified in this article in order to describe the experimental procedure adequately. This identification is not intended to imply recommendation or endorsement by the

National Institute of Standards and Technology, nor is it intended to imply that the items identified are the best available for the purpose.

[11] *Kwikweld*, J-B Weld Company LLC, Sulphur Springs, TX, U.S.A.

[12] Thorpe, James I., K. Numata, and J. Livas, *Optics Express* **16**, 15980-15990 (2008).

[13] R. W. P. Drever, J. L. Hall, F. V. Kowalski, J. Hough, G. M. Ford, A. J. Munley, and H. Ward, *App. Phys. B.: Photophys. Laser Chem.* **31**, 97-105 (1983).

[14] R. V. Pound, *Rev. Sci. Instrum.* **17**, 490-505 (1946).

[15] M. Puchalski, K. Piszczatowski, J. Komasa, B. Jeziorski, and K. Szalewicz, *Phys. Rev. A* **93**, 032515 (2016).